Inorganic Chemistry

ARTICLE

pubs.acs.org/IC

Photophysical Properties of Charged Cyclometalated Ir(III) Complexes: A Joint Theoretical and Experimental Study

Rubén D. Costa,[†,§] Filippo Monti,[‡] Gianluca Accorsi,[*,‡] Andrea Barbieri,[‡] Henk J. Bolink,[†] Enrique Ortí,[*,†] and Nicola Armaroli[‡]

[†]Instituto de Ciencia Molecular, Universidad de Valencia, 46980 Paterna (Valencia), Spain

[‡]Molecular Photoscience Group, Istituto per la Sintesi Organica e la Fotoreattività, Consiglio Nazionale delle Ricerche, Via P. Gobetti 101, 40129, Bologna, Italy

ABSTRACT: The photophysical properties of a series of charged biscyclometalated $[Ir(ppy)_2(N^{\wedge}N)]^{1+}$ complexes, where ppyH is 2-phenylpyridine and N^N is 2,2′-bipyridine (bpy), 6-phenyl-2,2′-bipyridine (pbpy), and 6,6′-diphenyl-2,2′-bipyridine (dpbpy) for complexes **1**, **2**, and **3**, respectively, have been investigated in detail. The photoluminescence performance in solution decreases from **1** to **3** upon attachment of phenyl groups to the ancillary ligand. The absorption spectra recorded over time suggest that complex **3** is less stable compared to complexes **1** and **2** likely due to a nucleophilic-assisted ancillary ligand-exchange reaction. To clarify this behavior, the temperature dependence of the experimental intrinsic deactivation rate constant, $k_{in} = 1/\tau$, has been investigated from 77 K to room temperature. Temperature-dependent studies show that nonemitting metal-centered (MC) states are accessible at room temperature for complex **3**. The experimental results are interpreted with the help of theoretical calculations performed within the density functional theory (DFT) approach. Calculations suggest that attachment of a phenyl group to the ancillary ligand (**2**) promotes the temperature-independent deactivation pathways, whereas attachment of a second phenyl group (**3**) also makes the temperature-dependent ones accessible through population of nonradiative ^{3}MC excited states.

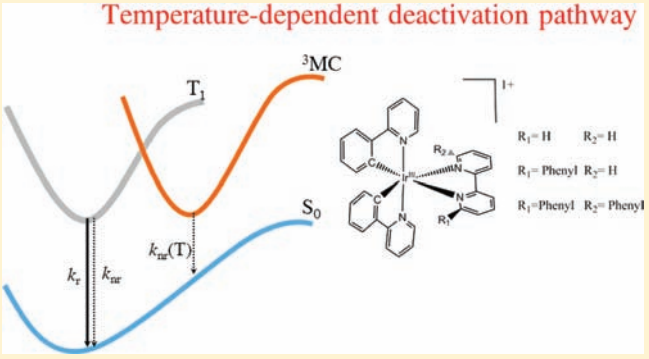

INTRODUCTION

Coordination complexes derived from second- and third-row transition-metal ions have been extensively studied in the last five decades. Preparation of d^6 isoelectronic transition-metal complexes (TMCs) using Ru(II), Os(II), or Ir(III) as the metal core has been found particularly attractive because of their strong metal−ligand interaction and high luminescence efficiencies.[1−3] Due to these characteristics, homoleptic and heteroleptic TMCs combining ancillary ligands (N^N), such as ethylenediamine (en), 2,2′-bipyridine (bpy), 1,10-phenanthroline (phen), etc., with cyclometalated ligands (C∧N), such as 2-phenylpyridine (Hppy), 1- phenylpyrazole (Hppz), etc., are excellent candidates for metal-ion sensing,[4−6] oxygen detection,[7] and lighting applications such as organic light-emitting diodes (OLEDs) and light-emitting electrochemical cells (LECs).[8−11]

LEC devices using ionic transition-metal complexes (iTMCs) as emitters have been extensively investigated since 1996.[9,12,13] The simplest LEC consists of a single active layer composed entirely of an iTMC balanced by small mobile counter anions such as $[PF_6^-]$ or $[BF_4^-]$. LECs are therefore based on only one active component, the iTMC, which simultaneously satisfies the requirements of electronic transport, luminescence, and ionic conduction, making them one of the simplest electroluminescent devices to date. Additionally, due to their operation mechanism, air-stable electrodes can be used, allowing for less rigorous encapsulation. All these characteristics make industrial production of LECs particularly attractive.

Since 2004 many breakthroughs concerning color gamut, efficiency, turn-on time, and stability in iTMC-based LECs LECs have been achieved using heteroleptic Ir(III) complexes,[14] hereafter abbreviated as Ir−iTMCs.[9,15−35] In their simplest form, the Ir−iTMCs used in LECs consist of a combination of at least two different ligands, two negatively charged cyclometalated C∧N ligands (such as Hppy or Hppz) and one neutral N^N ancillary ligand (such as bpy or phen), leading to a total charge of the complex of +1 (Figure 1). As LECs are based on only one active material, the most important enhancements concerning the performance of the device have been obtained by an appropriate tuning of the photophysical and electrochemical properties of the iTMCs. Some examples are (i) the highly efficient LECs achieved through attachment of bulky groups to the periphery of the Ir−iTMCs, which increase the photoluminescence quantum yield in film due to reduction of the self-quenching,[25,26,36,37] (ii) the blue-emitting LECs obtained by using Ir−iTMCs with ancillary ligands possessing a high-energy lowest-unoccupied molecular orbital (LUMO) and/or a deep highest-occupied

Received: April 20, 2011
Published: July 05, 2011

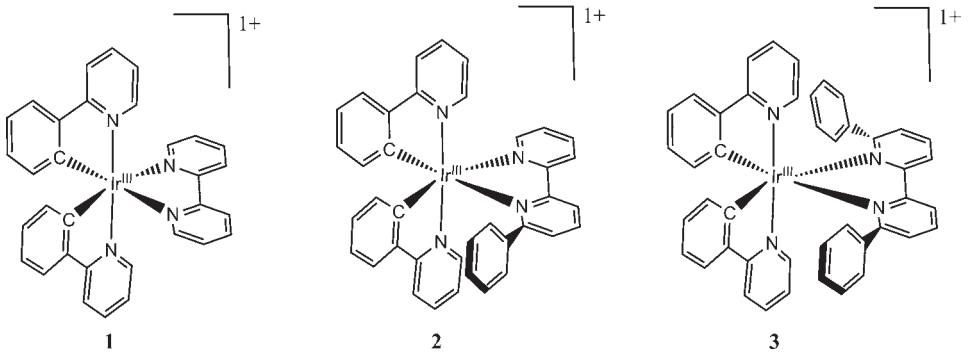

Figure 1. Chemical structures of the cations present in the Ir(III) complexes (**1**−**3**) studied in this paper.

molecular orbital (HOMO) due to introduction of electron-withdrawing groups on the cyclometalated ligand,[17,23,29,30,32] and (iii) LECs with stability in excess of 1000 h by using supramolecularly caged Ir−iTMCs as the single active component.[15,16,21,26,27,33]

Although the last breakthroughs achieved for LECs mostly result from a thorough tuning of the photophysical properties of the Ir−iTMCs, there are only a few works in which the photophysics of these complexes is studied in detail.[1−3,38−45] This knowledge is of the upmost importance to design efficient and stable emitters. In the present paper, we investigate the photophysical properties of a series of Ir−iTMCs used in LECs by studying the temperature dependence of the emission properties and by performing theoretical DFT calculations. The series consists of the archetype complex $[Ir(ppy)_2(bpy)][PF_6]$ (**1**) and the supramolecularly caged complexes $[Ir(ppy)_2(pbpy)][PF_6]$ (**2**) and $[Ir(ppy)_2(dpbpy)][PF_6]$ (**3**), where pbpy is 6-phenyl-2,2′-bipyridine and dpbpy is 6,6′-phenyl-2,2′-bipyridine (Figure 1). Although attachment of phenyl groups leads to highly stable LEC devices, it causes a decrease of the device efficiency especially when using complex **3**.[21] With this study we identified potential deactivation pathways of a series of charged iridium complexes and show that in some cases the temperature-dependent deactivation via population of nonradiative metal-centered (^{3}MC) excited states is feasible.

EXPERIMENTAL PROCEDURES

Spectroscopic Measurements. Absorption spectra were recorded with a Perkin-Elmer Lambda 950 spectrophotometer. For photoluminescence experiments, the samples were placed in fluorimetric 1 cm path cuvettes and purged from oxygen by bubbling with argon. Uncorrected emission spectra were obtained with an Edinburgh FLS920 spectrometer equipped with a Peltier-cooled Hamamatsu R928 photomultiplier tube (185−850 nm). An Edinburgh Xe900 450 W xenon arc lamp was used as the excitation light source. Corrected spectra were obtained via a calibration curve supplied with the instrument. Photoluminescence quantum yields (Φ_{PL} or PLQY) in solution were obtained from corrected spectra on a wavelength scale (nm) and measured according to the approach described by Demas and Crosby[46] using air-equilibrated $[Ru(bpy)_3][Cl]_2$ water solution ($\Phi_{PL} = 0.028$)[47] as standard. Excited-state lifetimes (τ) were determined with the single-photon counting technique by means of the same Edinburgh FLS920 spectrometer using a laser diode as the excitation source ($\lambda_{exc} = 407$ nm) and the above-mentioned PMT as the detector. Analysis of the luminescence decay profiles vs time was accomplished with the Decay Analysis Software provided by the Edinburgh FLS920 manufacturer, and the quality of the fit was assessed by the χ^2 value close to unity with the residuals regularly distributed along the time axis. To record the 77 K luminescence spectra, the samples were put in quartz tubes (2 mm inner diameter) and inserted in a special quartz Dewar flask filled up with liquid nitrogen. Solid sample films consist of a pure layer of spin-coated compound from a concentrated (20 mg/mL) dichloromethane solution deposited on a flat quartz support. Solid-state Φ_{PL} values were calculated by corrected emission spectra obtained from an Edinburgh FLS920 spectrometer equipped with a barium sulfate-coated integrating sphere (diameter of 4 in.) following the procedure described by De Mello et al.[48] For temperature-dependence measurements, all samples (oxygen-free methanol/ethanol solutions, 1:4 v/v) were sealed under vacuum in a 1 cm fused quartz cell. This cuvette was placed inside a modified C600 Thor cryostat filled with liquid nitrogen (operating range 90−400 K) and equipped with a 3050 Thor temperature controller. Experimental uncertainties are estimated to be ±8% for τ determinations, ± 20% for PLQYs, ± 2 and ±5 nm for absorption and emission peaks, respectively, and ±2 K for the temperature in the cryostat.

Computational Details. Density functional theory calculations (DFT) were carried out with the A.01 revision of the Gaussian 09 program package[49] using Becke's three-parameter B3LYP exchange-correlation functional[50−52] together with the 6-31G** basis set for C, H, and N atoms[53] and the "double- ζ" quality LANL2DZ basis set for the Ir element.[54] An effective core potential (ECP) replaces the inner core electrons of Ir leaving the outer core $[(5s)^2(5p)^6]$ electrons and the $(5d)^6$ valence electrons of Ir(III). The molecular structures of the complexes in the singlet ground state (S_0), the lowest triplet excited state (T_1), and the metal-centered (^{3}MC) triplet excited states were fully optimized in dichloromethane. Triplet states were calculated at the spin-unrestricted UB3LYP level with a spin multiplicity of 3. The expected values calculated for S^2 were always smaller than 2.05. Solvent effects were considered within the SCRF (self-consistent reaction field) theory using the polarized continuum model (PCM) approach to model the interaction with the solvent.[55,56]

RESULTS AND DISCUSSION

Molecular and Electronic Structures: Ground-State Characterization by DFT Calculations. The molecular and electronic structures of complexes **1**−**3** were investigated by DFT calculations at the B3LYP/(6-31G**+LANL2DZ) level considering solvent effects (see the Experimental Section for details). The geometries of the complexes in the electronic ground state (S_0) were fully optimized, and the values obtained for selected bond lengths and dihedral angles are listed in Table 1. Theoretical values compare well with the X-ray data reported for the three complexes.[15,21,22] The Ir−C and Ir−N bond distances together with the dihedral $N_{bpy}-C-C-N_{bpy}$ angle of the ancillary ligand calculated for **1** suggest a near-octahedral

dx.doi.org/10.1021/ic200820t |*Inorg. Chem.* 2011, 50, 7229–7238

Table 1. Selected Bond Distances (Å) and Dihedral N−C−C−N Angle (deg) of the bpy Ligand Calculated for the Cations of Complexes 1, 2, and 3 in the S_0 Ground State and in the T_1 and Metal-Centered (^{3}MC) Triplet Excited States

complex	distance/angle	X-ray[a]	S_0	T_1	^{3}MC
1	Ir−C_{ppy}	2.01	2.024	1.999	2.015
	Ir−N_{ppy}	2.05	2.082	2.081	2.505
	Ir−N_{bpy}	2.13	2.210	2.196	2.219
	N_{bpy}−C−C−N_{bpy}	2	4.9	1.5	1.0
2	Ir−C_{ppy}	2.00/2.03	2.013/2.028	2.018/1.985	2.042/2.033
	Ir−N_{ppy}	2.04/2.07	2.093/2.079	2.087/2.076	2.604/2.204
	Ir−N_{bpy}	2.15/2.22	2.360/2.207	2.238/2.226	2.515/2.226
	N_{bpy}−C−C−N_{bpy}	18.4	17.6	11.6	19.1
3	Ir−C_{ppy}	2.01	2.021/2.019	2.011/1.990	2.050/2.030
	Ir−N_{ppy}	2.05/2.03	2.081/2.075	2.096/2.071	2.614/2.209
	Ir−N_{bpy}	2.23/2.20	2.345/2.355	2.233/2.301	2.503/2.305
	N_{bpy}−C−C−N_{bpy}	20.7	36.0	6.0	33.5

[a] X-ray values were taken from the refs 22 (**1**), 15 (**2**), and 21 (**3**).

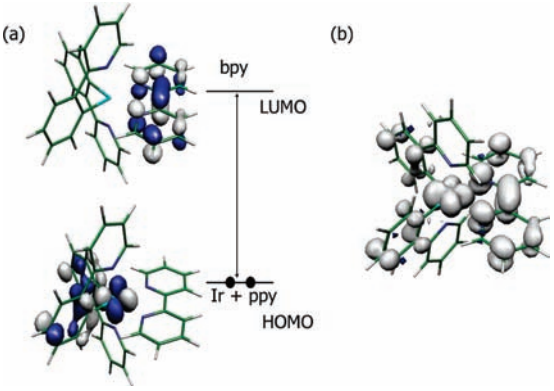

Figure 2. (a) Schematic diagram showing the electronic density contours (0.05 e bohr^{-3}) calculated for the frontier molecular orbitals of complex **1**. (b) Spin density distribution (0.005 e bohr^{-3}) calculated for the emitting excited state (T_1) of complex **1**.

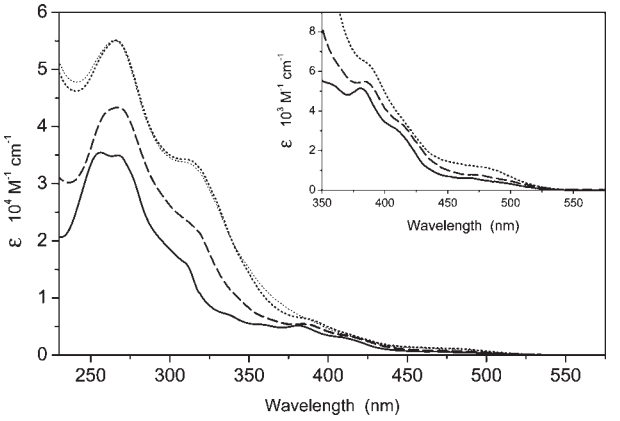

Figure 3. Electronic absorption spectra of complexes **1** (solid), **2** (dashed), and **3** (thick dotted) in DCM solution at room temperature; MLCT transitions are zoomed in the inset. The absorption spectrum of **3** recorded after 24 h is reported as thin dots; those of **1** and **2** are unchanged.

coordination of the iridium metal core. Complexes **2** and **3** show a more distorted octahedral coordination owing to the sequential attachment of phenyl groups to the 6- and 6′-positions of the bpy ligand (Figure 1 and Table 1). For both complexes, the pendant phenyl rings exhibit an intracation face-to-face π-stacking interaction with the phenyl rings of the cyclometalated ligands (calculated centroid−centroid distances of ∼3.60 Å). As a consequence of this interaction, the Ir−N_{bpy} distances of the phenyl-substituted pyridine rings lengthen from 2.21 Å in **1** to 2.35−2.36 Å in **2** and **3** and the N_{bpy}−C−C−N_{bpy} dihedral angle gradually increases from 4.9° (**1**) to 17.6° (**2**) and 36.0° (**3**) (Table 1). Indeed, complex **3** shows a strongly distorted molecular structure in which the ancillary ligand can be considered to be partially decoordinated from the iridium metal core. Hence, complex **3** seems to be less robust in both the ground and the excited states, which increases the possibility for nucleophilic-assisted ancillary ligand-exchange reactions, leading to degradation of the complex. This behavior has been also observed in other comparable iridium complexes by Neve et al.[42]

Figure 2 displays the atomic orbital composition calculated for the HOMO and LUMO of complex **1**. The same composition of the frontier molecular orbitals is obtained for complexes **2** and **3**. As already reported for analogous cyclometalated Ir−iTMCs,[22,38,39,57] the HOMO is composed of a mixture of Ir(III) d_π orbitals (t_{2g}) and phenyl π orbitals of the ppy ligands and the LUMO resides on the ancillary ligand (Figure 2a). Upon introduction of phenyl groups on the ancillary ligand, the energy of the HOMO remains almost constant (−5.83, −5.82, and −5.82 eV for **1**, **2**, and **3**, respectively), whereas the LUMO is gradually destabilized (−2.65, −2.61, and −2.46 eV for **1**, **2**, and **3**, respectively). The destabilization of the LUMO is ascribed to the distortion of the ancillary ligand caused by the π-stacking interaction between the pendant phenyl rings and the cyclometalated ligands. As discussed above, this interaction determines a progressive increase of the internal torsional angle of the ancillary ligand (Table 1), which reduces the conjugation between the pyridine rings with a consequent destabilization of the LUMO level and weakens the metal−ligand bond.

Absorption and Emission Spectroscopy: Characterization of the Emitting Excited State. The electronic absorption spectra of complexes **1**−**3** were recorded at room temperature (RT) in dichloromethane (DCM) solution (see Figure 3). The UV region (250−350 nm) is dominated by intense absorption bands ($\varepsilon \approx 10-55 \times 10^3$ M^{-1} cm^{-1}) that are assigned to

dx.doi.org/10.1021/ic200820t |Inorg. Chem. 2011, 50, 7229–7238

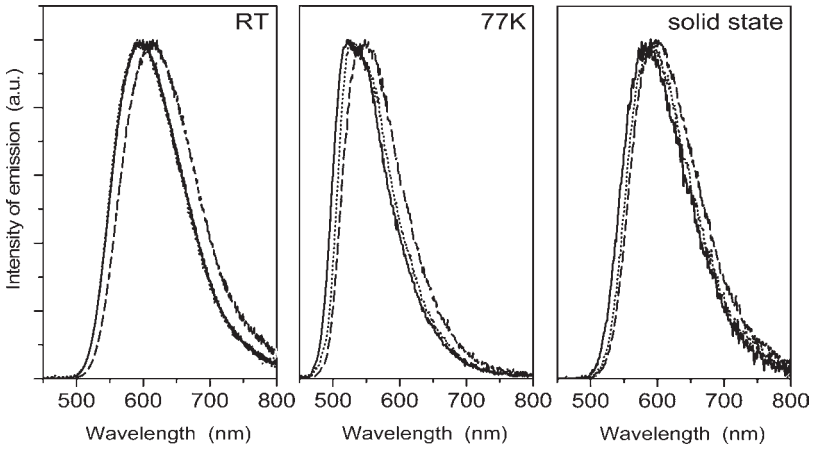

Figure 4. Normalized emission spectra of **1** (solid), **2** (dashed), and **3** (dotted) in room-temperature DCM solution (left), 77 K DCM frozen matrix (middle), and pure solid-state spin-coated thin film (right). λ_{exc} = 407 nm (the emission profiles of complexes **1** and **3** at room temperature are almost superimposed).

Table 2. Photophysical Properties in DCM Solution (RT and 77 K) and in Thin Film (RT)

	DCM at RT[a]					DCM at 77 K[a]		thin film[b]		
	λ_{max} (nm)	Φ_{PL} (%)	τ (ns)	k_r (10^5 s^{-1})	k_{nr} (10^6 s^{-1})	λ_{max} (nm)	τ (μs)	λ_{max} (nm)	Φ_{PL} (%)	τ (ns)
1	595	19.6	565	3.5	1.4	521	3.5	582	20	587
2	614	4.9	204	2.4	4.7	548	2.6	598	12	364
3	594	3.6	131	2.7	7.4	528	4.3	593	17	505

[a] Emission maxima in oxygen-free solution from corrected spectra, λ_{exc} = 407 nm. [b] As pure compound, spin coated from 20 mg/mL DCM solutions, λ_{exc} = 407 nm.

spin-allowed ligand-centered (LC) $\pi-\pi^*$ transitions involving both the cyclometalated and the ancillary ligands. On the other hand, the weak and broader bands ($\varepsilon \approx 1-9 \times 10^3$ M^{-1} cm^{-1}) at longer wavelengths (350−450 nm) are attributed to charge transfer transitions with mixed metal-to-ligand (^{1}MLCT) and ligand-to-ligand (^{1}LLCT) charge transfer character (Figure 3, inset).[38,39,58,59] Additionally, the weak and long tail observed in the spectra above 450 nm is due to direct spin-forbidden absorption from the singlet ground state to the triplet excited states enabled by the high spin−orbit coupling constant of the iridium metal core (ζ_{Ir} = 3909 cm^{-1}).[3] The presence of phenyl substituents on the bipyridine ligand leads both to red spectral shifts and to higher molar extinction coefficients (**1** < **2** < **3**).

The absorption spectra of complexes **1**−**3** were recorded over time to investigate the effects of the gradual distortion of the coordination sphere on the stability of the complex upon attachment of the phenyl groups. Figure 3 compares the absorption profiles obtained from fresh DCM solutions (thick lines) with those after 24 h in the dark (thin lines). While the absorption profiles recorded over time (24 h) for **1** and **2** are completely superimposed, those of **3** show small spectral shifts and changes in intensity, suggesting a lower stability. Indeed, after several days the absorption profile of **3** is remarkably different compared to that from fresh solution, while those of complexes **1** and **2** remain unaltered. From further studies in other solvents, it can be stated that **1** and **2** are stable over weeks, even in highly coordinating solvents such as acetonitrile or methylethylketone, while complex **3** shows rather rapid degradation (depending on the nucleophilicity of the solvent). Time-dependent absorption spectra therefore evidence the poor stability of complex **3**, which is likely attributed to nucleophilic-assisted ancillary ligand-exchange reactions due to partial decoordination of the ancillary ligand caused by attachment of phenyl rings on the 6- and 6′-positions.

Photoluminescence studies in different conditions were performed to elucidate the effect of phenyl substitution on the photophysical properties of complexes **1**−**3**. Figure 4 displays the emission spectra in DCM solution at room (RT) and at low temperature (77 K) together with those recorded for pure solid-state thin films at 298 K. The corresponding PL data are collected in Table 2. Luminescence decays are in the tenths-of-microsecond scale, indicating a phosphorescence process. This is very common in cyclometalated Ir(III) complexes as the intersystem crossing process is very fast and leads to near quantitative triplet formation.[1−3] Passing from solution to the pure thin film and, finally, to the low-temperature rigid matrix, a progressive blue shift of the emission band occurs for all complexes (Table 2). This trend is in line with the stabilizing effect on the lowest triplet excited state exerted by the different environments (77 K rigid-matrix < RT solid state < RT solution)[60] and indicates that the emitting excited state has a strong charge transfer (CT) character. The broad and structureless shape of the emission profiles and the radiative constants ($2.4 \times 10^5 < k_r < 3.5 \times 10^5$ s^{-1}, Table 2) observed for the three complexes also corroborate this hypothesis (Figure 4).

To obtain a more detailed description of the nature of the emitting triplet state, DFT calculations at the unrestricted UB3LYP level were used to fully optimize the electronic and

molecular structures of the lowest triplet state (T_1) in the presence of the solvent. The T_1 state mainly results from the HOMO → LUMO monoexcitation and is computed to lie 2.34 (**1**), 2.31 (**2**), and 2.38 eV (**3**) above S_0 (adiabatic energy differences). Excitation to T_1 hence implies an electron transfer from the Ir−ppy environment to the ancillary ligand. This is illustrated in Figure 2b by the unpaired-electron spin density distribution calculated for complex **1**, which perfectly matches the topology of the HOMO → LUMO excitation (Figure 2a) in which the T_1 state originates. For the three complexes, the spin densities calculated for T_1 are very similar (Ir 0.50, ppy 0.48, and bpy 1.10 for **1**, Ir 0.49, ppy 0.45, and pbpy 1.06 for **2**, and Ir 0.50, ppy 0.42, and dpbpy 1.08 for **3**) and confirm a mixed metal-to-ligand and ligand-to-ligand charge transfer (^{3}MLCT/^{3}LLCT) nature of the emitting triplet state. The phosphorescence emission energy can be correlated with the vertical energy difference between T_1 and S_0 estimated by performing a single-point calculation of S_0 at the optimized minimum-energy geometry of T_1. Calculations lead to vertical emission energies of 2.06 eV (602 nm) for **1**, 1.98 eV (626 nm) for **2**, and 2.00 eV (620 nm) for **3**, in good agreement with the experimental λ_{max} values in solution (Table 2). Note that independent of the experimental conditions, the emission profiles of **2** show a small red shift compared to those of **1** and **3** (Figure 4). The adiabatic and vertical energy differences calculated for T_1 support this trend.

In DCM solution, the luminescence performance of this series of compounds worsens on going from **1** to **3** (Table 2). Complex **1** shows an emission intensity (Φ_{PL} = 0.20) and a lifetime (τ = 565 ns) substantially greater than those of **2** and **3**, which leads to the smallest nonradiative rate constant value (1.4×10^6 s^{-1}). Overall, deactivation of the emitting excited states in d^6 transition-metal complexes follows three main processes.[1−3] (i) An almost temperature-independent nonradiative process, with kinetic rate constant k_{nr}, which usually occurs through direct potential energy surface crossing and/or vibrational coupling between T_1 and S_0 states. (ii) A minor temperature-dependent radiative process, with kinetic rate constant $k_r(T)$, related to the thermal population of the individual triplet substates of T_1 (T_I, T_{II} and T_{III}), each of which has a unique radiative decay rate. For transition-metal complexes having significant contributions of MLCT character in their emitting excited state, the zero-field splitting (zfs) generally is of a few hundred cm^{-1}.[61−63] Thermal equilibration of the individual triplet sublevels is therefore effective at T > 77 K, and phosphorescence can be treated as originating from a single state, having an average k_r = 1/3 [$k_r(T_I)$ + $k_r(T_{II})$ + $k_r(T_{III})$]. For practical purposes, both (i) and (ii) can be regarded as temperature-independent processes. (iii) A temperature-dependent nonradiative process, with kinetic rate constant $k_{nr}(T)$, comprising the thermal population of higher-lying nonradiative excited states, e.g., ^{3}MC states, frequently associated with an activation energy barrier. Similar schemes have been proposed for neutral Ir(III) complexes and for charged Ru(II) and Os(II) complexes.[1,3,61,64] According to most investigated cases, the clusters of MLCT and MC states can be considered as single MLCT and MC levels. A detailed study of the temperature dependence of the global deactivation rate constant is presented in the next section for complexes **1**−**3**.

Following this general scenario, the stronger luminescence observed for complex **1** compared to **2** and **3** (Table 2) suggests that **1** shows less effective nonradiative deactivation pathways. To confirm this notion, we correlate the structural changes predicted in passing from S_0 to T_1 with the temperature-independent deactivation (k_{nr}) pathway in a qualitative way.[1,3,65−67] The electron transfer associated with the excitation to the T_1 state causes a similar contraction of the coordination sphere for the three complexes (Table 1). However, complex **1** shows less-pronounced geometrical changes in passing to T_1 compared to **2** and **3**, which suggests that the temperature-independent deactivation pathway should be less effective than in the other two complexes. For complex **2**, the main structural changes upon excitation to T_1 are (i) the Ir−N_{bpy} distance of the phenyl-substituted pyridine ring is strongly shortened (0.12 Å) with respect to that calculated for S_0 and (ii) the ancillary ligand suffers a flattering of 6°. These structural changes favor the temperature-independent nonradiative decay associated to vibrational deactivations and can be one of the reasons that explain the higher k_{nr} value obtained for **2** (Table 2).[1,3,65−67] A second factor that contributes to the better photophysical properties of **1** is the slightly higher energy of the T_1 emitting state compared to **2** (Table 2), which favors radiative deactivation according to the energy gap law.[68] A further reason to be considered for explaining the k_{nr} of **2** is the population of thermally accessible nonradiative excites states ($k_{nr}(T)$) which is studied in detail in the next section. For complex **3**, a stronger flattering process (30°) occurs in T_1 (Table 1) and more effective vibrational deactivations should be expected in accordance with the higher value obtained for k_{nr} (Table 2). However, other deactivation pathways can be likely present in **3** as the Ir−N_{bpy} distance of one pyridine ring of the ancillary ligand is significantly longer (0.07 Å) than those of complexes **1** and **2**. The weakness of the Ir−N_{bpy} bond suggests that **3** could present an effective luminescence quenching process of the T_1 state through nucleophilic-assisted ligand-exchange processes and/or population of thermally accessible nonradiative states ($k_{nr}(T)$). This hypothesis is corroborated by the low stability shown by **3** in the absorption studies discussed above.

Further information to support the above-mentioned hypothesis is obtained from photoluminescence studies at low temperature (77 K rigid matrix) and in thin films. At 77 K, the PLQY is difficult to measure with acceptable accuracy but the observed lifetime can provide quantitative information thanks to the good correlation between the luminescence intensity and the relative decay.[69] The long lifetimes (microseconds time scale, Table 2) measured under such conditions indicate appreciable photoluminescence performances for the three complexes. The lifetime of **3** (4.3 μs) suffers the largest change and is the longest of the series at 77 K, supporting the hypothesis that nucleophilic-assisted ligand-exchange processes and/or population of thermally accessible nonradiative states are present in RT solution, mainly for this complex. This hypothesis is further reinforced by the photophysical data in the solid state. In fact, whereas the PLQY of **1** remains unchanged in passing from solution to solid state (Table 2), complexes **2** and **3** exhibit higher quantum yields and significantly longer lifetimes. The changes are more pronounced for complex **3** (Φ_{PL} = 0.17, τ = 505 ns), which shows a luminescence intensity almost 5 times higher in a rigid environment than in the presence of solvent molecules. This suggests that the deactivation pathways are reduced in rigid matrix.

Temperature Dependence of Emission Lifetimes: Following the Deactivation Pathways. As discussed above, one of the factors determining the change of the nonradiative constant with complexes **1**−**3** is the enhancement of the temperature-independent nonradiative processes. However, they can also present other deactivation pathways related to the population

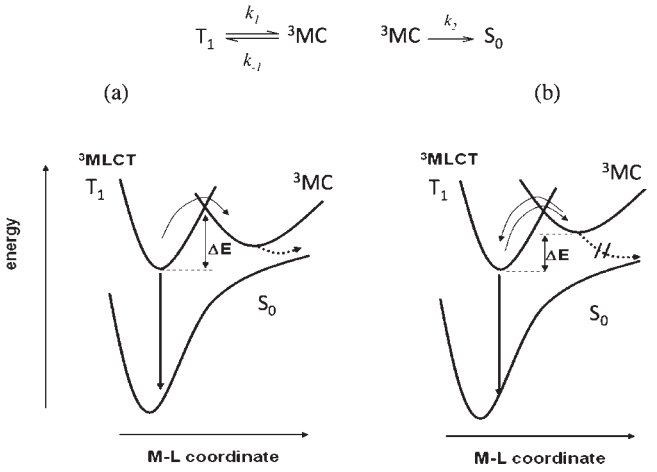

Figure 5. Potential energy curves illustrating two kinetic cases (a and b) for the involvement of ^{3}MC states in the deactivation of the emitting excited state T_1.

of thermally accessible nonradiative states, $k_{nr}(T)$. This behavior is very common in d^6 transition-metal complexes based on Ru(II), Os (II), and Ir(III) metal cores.[1,3,61,64] For this type of complexes, a temperature dependence of k_{nr} has been observed and higher-lying, thermally accessible and reactive levels of ^{3}MC nature have proven to play an important role in photophysical patterns.[1,3,61,64] On a general ground, deactivation of the emitting excited state (T_1) is related to an activated surface crossing from the T_1 manifold to a higher-lying ^{3}MC level, which subsequently undergoes a nonradiative deactivation to the ground state S_0 (Figure 5).

Key information about the population of thermally accessible nonradiative states can be obtained by studying the temperature dependence of the experimental intrinsic deactivation rate constant, $k_{in} = 1/\tau$, where τ is the excited-state lifetime. The temperature dependence of k_{in} can be accounted for by the equation[70]

$$k_{in}(T) = k_0 + \frac{B}{1 + exp[C(T^{-1} - T_g^{-1})]} + \sum_i A_i \, exp(-\Delta E_i/RT) \quad (1)$$

where k_0 is a temperature-independent term, the second term takes care empirically of the effect of the rigid−fluid transition, and the third term is the usual Arrhenius expression which contains a frequency factor, A_i, and an activation barrier, ΔE_i. In Figure 6, a graphical representation of eq 1 is displayed, in which the contribution of each single term has been separated and highlighted. In particular, the second term describes a stepwise behavior centered at the rigid−fluid transition temperature T_g, where C is related to the smoothness of the step and B is the value achieved by $T \rightarrow 0$ (for a detailed discussion see ref 70), while the slope of the green and blue curves is related to the activation energy ΔE_i of the ith process. Once the ^{3}MC state is populated, two limiting kinetic cases can be expected: (a) when a strong coupling of the ^{3}MC level with the S_0 state takes place ($k_2 \gg k_{-1}$; Figure 5a), the frequency factor is predicted to be large, $A > 10^{10}$ s^{-1}, and ΔE is the activation energy barrier between the emitting level and the ^{3}MC state and (b) when $k_{-1} \gg k_2$ (Figure 5b), the frequency factor is predicted to be

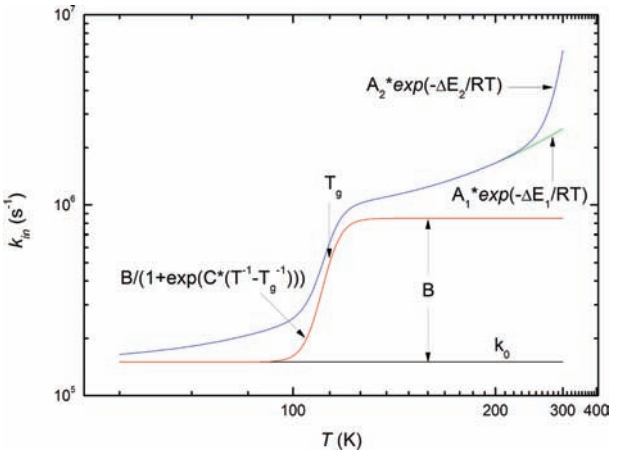

Figure 6. Graphical representation of the fitting function used, highlighting the contribution of the different terms in eq 1 and the physical meaning of some parameters.

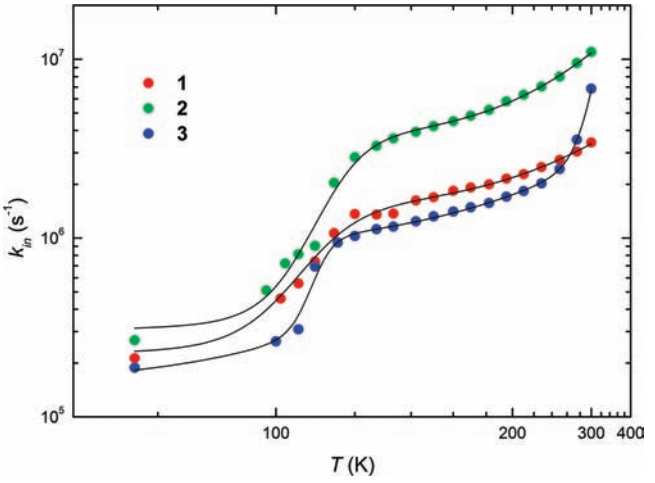

Figure 7. Temperature-dependent luminescent decay, as $k_{in} = 1/\tau$, of complexes **1**, **2**, and **3**. The lines are the fitting curves of the data using eq 1 with two Arrhenius terms and the parameters reported in Table 3.

$<10^8$ s^{-1} and ΔE is the energy separation between the emitting level and the ^{3}MC state.[70]

In order to gain an understanding of the role played by thermally activated nonradiative decay processes on the luminescence properties of complexes **1**−**3**, temperature-dependent experiments were undertaken from 77 K to room temperature in degassed MeOH/EtOH 1:4 solution. Figure 7 displays the evolution of the k_{in} deactivation rate constant as a function of temperature. Table 3 summarizes the values obtained for the k_0, A_i, ΔE_i, B, C, and T_g parameters from the nonlinear iterative fitting of k_{in} data as a function of temperature using eq 1 with two Arrhenius terms. The related error is reported beside each parameter, together with the corresponding chi-squared factor, χ^2.

The temperature-independent term k_0, which has a similar value for all the complexes ($\sim 2 \times 10^5$ s^{-1}), is comparable to the radiative constant ($k_r = \Phi_{PL}/\tau$) obtained from data at room temperature (Table 2). The three complexes under investigation show a quite similar stepwise term in the temperature range $100 < T < 120$ K, with $B \approx 10^6$ s^{-1}, $C \approx 2-4 \times 10^3$, and T_g in the range 110−116 K (Table 3). This second term in eq 1

dx.doi.org/10.1021/ic200820t |Inorg. Chem. 2011, 50, 7229–7238

Table 3. Kinetic Parameters for Excited-State Decay Obtained from Temperature-Dependent Measurements

complex	k_0 (s^{-1})	B (s^{-1})	C (K)	T_g (K)	A_1 (s^{-1})	ΔE_1 (cm^{-1})	A_2 (s^{-1})	ΔE_2 (cm^{-1})	χ^2
1	2.2×10^5	1.22×10^6	1.64×10^3	111.8	1.30×10^7	400			0.9982
2	3.0×10^5	3.30×10^6	2.10×10^3	116.3	7.60×10^7	490			0.9991
3	1.5×10^5	0.71×10^6	4.5×10^3	110.0	0.74×10^7	300	7×10^{12}	3000	0.9997

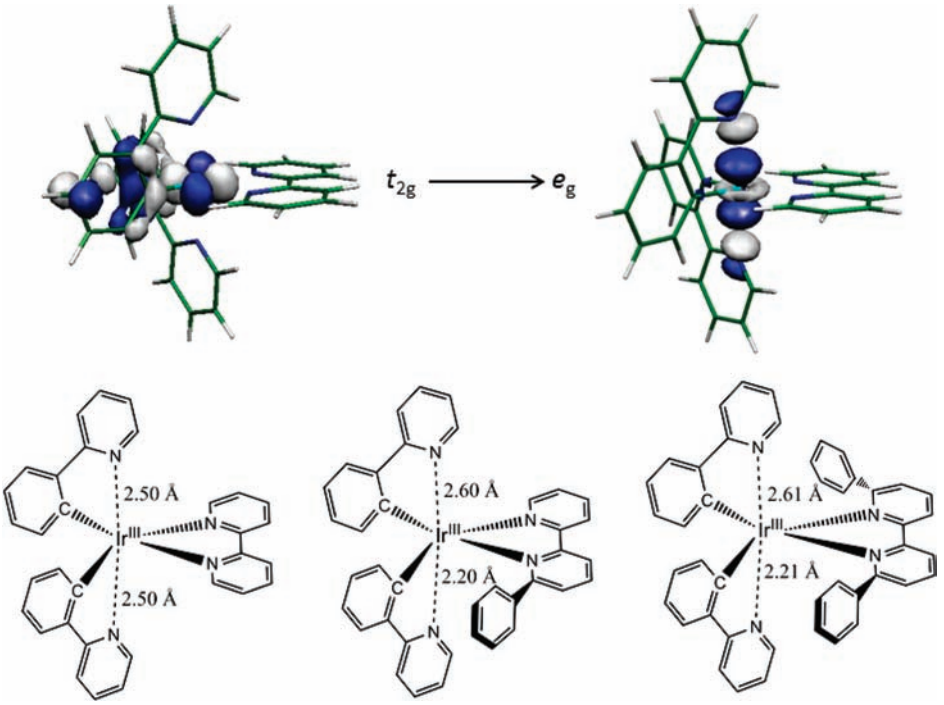

Figure 8. (Top) Electron density contours (0.05 e $bohr^{-3}$) calculated for the occupied t_{2g} and unoccupied e_g molecular orbitals of complex **1**. The e_g orbital shows σ-antibonding interactions along the vertical $N_{ppy}-Ir-N_{ppy}$ axis. (Bottom) Sketch of the molecular structure calculated for the ^{3}MC state of complexes **1** (left), **2** (middle), and **3** (right).

corresponds to the red shift observed in the emission maxima of all complexes in the same temperature range and is associated with small rearrangements of the solvent molecules on softening of the solvent matrix and/or with reorientation of the solvent dipoles to arrange the charge displacement induced in the emitting excited state of these complexes. Solvent reorganization can only take place when the solvent has acquired the properties of a nonviscous fluid, i.e., here at $T > 120$ K. Plots of the intrinsic decay rate, $k_{in} = 1/\tau$, at temperatures higher than 120 K display two distinct regimes (Figure 7): one at low temperature ($120 < T < 220$ K) that corresponds to thermal redistribution between the triplet sublevels (dependent on the zfs) and the other at higher temperature ($T > 250$ K) that involves population of the nonradiative ^{3}MC state. Complexes **1**−**3** display a low-temperature activation, which corresponds to the thermal redistribution between the triplet sublevels, as suggested by the low value of the frequency factor ($A_1 \approx 10^7$ s^{-1}, Table 3). Accordingly, the $\Delta E_1 = 300-500$ cm^{-1} obtained represents the zfs between the T_I and T_{III} triplet substates. The smaller splitting between sublevels T_I and T_{II} could not be resolved in the temperature range analyzed. These ΔE values are in good agreement with results reported in the literature for similar complexes, where the zfs was found to range between 100 and 400 cm^{-1}.[1−3,61−63] Hence, the decrease in lifetime observed for the Ir(III) complexes under investigation upon warming from 120 to 240 K is due to thermal population of the higher triplet sublevels, particularly the T_{III} substate responsible for fast radiative decay. As the temperature increases ($T > 250$ K), a second Arrhenius term is needed to account for the temperature dependence of k_{in} of only complex **3**. In this case, the frequency factor $A_2 = 7 \times 10^{12}$ s^{-1} (Table 3) suggests that the value calculated for ΔE_2 (3000 cm^{-1}) represents the activation energy for population of a high-lying nonradiative ^{3}MC excited state (Figure 5a).

Metal-centered states result from excitation of an electron from the occupied t_{2g} ($d\pi$) HOMO to the unoccupied e_g ($d\sigma^*$) orbitals of the metal (Figure 8).[22,71] The geometry of the ^{3}MC states was fully relaxed starting from the optimized geometry of S_0 with $Ir-N_{ppy}$ bond distances lengthened to 2.70 Å since, as sketched in Figure 8, the e_g ($d\sigma^*$) orbital is σ-antibonding between the metal and the nitrogens of the ppy ligands. Electron promotion to this orbital however leads to different molecular structures for the ^{3}MC state of complexes **1**−**3** (Table 1). Whereas for complex **1** both $Ir-N_{ppy}$ distances lengthen to a value of 2.51 Å (2.08 Å in S_0), the intramolecular π-stacking interaction present in complexes **2** and **3** prevents the weakening of one of the $Ir-N_{ppy}$ bonds which lengthen to ∼2.60 and ∼2.20 Å (Figure 8). The pendant phenyl rings in 6- and 6′-positions thus exert a cage effect that restricts the opening of the structure of complexes **2** and **3** in the excited ^{3}MC state and only one of the N_{ppy} atoms is virtually decoordinated.

dx.doi.org/10.1021/ic200820t |*Inorg. Chem.* 2011, 50, 7229–7238

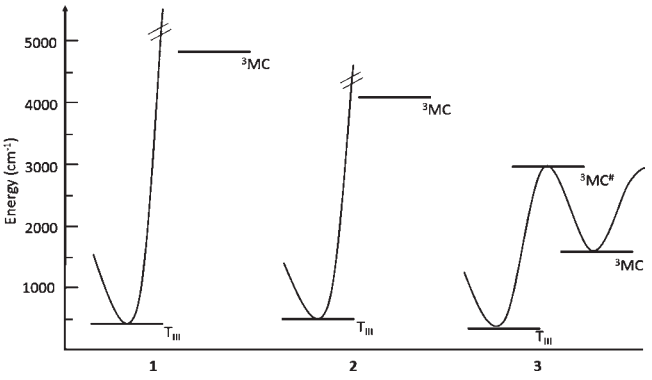

Figure 9. Excited-state energy level diagram with the lowest energy T_I emitting state set as zero (for the meaning of T_I and T_{III} see text). $^3MC^{\#}$ is the activation energy obtained from temperature-dependent experiment analysis (see text). The energies of the ^3MC states are the adiabatic energy differences with respect to the lowest-energy triplet excited state obtained from theoretical calculations.

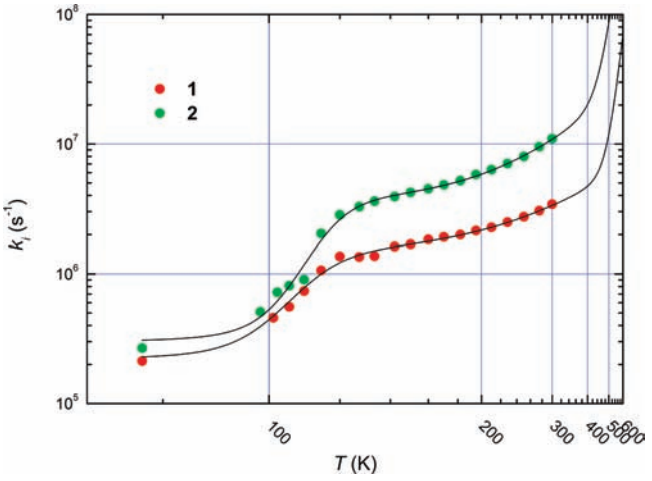

Figure 10. Fitting lines obtained using in eq 1 the relevant data given for complexes **1** and **2** in Table 3 but adding a second Arrhenius term with $A_2 = 7 \times 10^{12}$ s^{-1} and $\Delta E_2 = 4834$ and 4028 cm^{-1}, respectively.

After geometry relaxation, the ^3MC states of complexes **1** and **2** are calculated to lie at 0.60 (4834 cm^{-1}) and 0.50 eV (4028 cm^{-1}) above the lowest-energy T_1 state (adiabatic energy differences), respectively. In contrast, the ^3MC state of complex **3** is computed to be only 0.20 eV (1611 cm^{-1}) above the T_1 state. The energy diagram sketched in Figure 9 compares these theoretical energy differences with the energies obtained from the temperature-dependent analysis (Table 3) for the T_{III} energy levels (ΔE_1) and the ^3MC activation barrier (ΔE_2). In the case of complex **3**, the calculated ^3MC state is situated ~1400 cm^{-1} below the activation energy barrier ($^3MC^{\#}$, $\Delta E_2 = 3000$ cm^{-1}) deduced experimentally. Hence, the calculated and experimental data are in qualitative agreement. The ^3MC states of complexes **1** and **2** are situated higher in energy well above the emitting triplet state (>4000 cm^{-1}), and no thermal activation to the nonradiative excited states is observed in temperature-dependent experiments in the range $90 < T < 400$ K, which implies that they do not substantially participate in the deactivation of the T_1 emitting state. This suggests that the decrease in the photophysical performance observed in solution in passing from complex **1** to **2** (Table 2) is mainly related to an enhancement of the temperature-independent deactivation pathways. The situation is completely different for complex **3** where the population of the nonradiative ^3MC states is an efficient pathway for radiationless processes, corresponding to case a of Figure 5, as suggested by the high value of the frequency factor, $A_2 = 7 \times 10^{12}$ s^{-1} (Table 3).

A simulation conducted by using a second Arrhenius term with $A_2 = 7 \times 10^{12}$ s^{-1} and $\Delta E_2 = 4834$ and 4028 cm^{-1} for the fitting of k_{in} vs the temperature data obtained for complexes **1** and **2**, respectively, in analogy with the behavior observed for **3**, provides useful hints. The simulation curves are reported in Figure 10 (full lines) together with experimental data. It is evident that in order to observe a bending in the curves, indicative of an activation process, experiments should be conducted at $T > 450-500$ K, a temperature range not accessible with the useful solvents available for this type of Ir(III) complexes. This definitely rules out the possibility to experimentally observe in solution the population of the ^3MC states at the energies predicted by the theoretical calculations.

CONCLUSIONS

The photophysical properties of a series of charged biscyclometalated $[Ir(ppy)_2(bpy)]^+$ complexes, in which phenyl groups are sequentially attached to the 6- and 6′-positions of the bpy ligand, have been thoroughly studied by using both experimental and theoretical approaches. The photoluminescence properties measured in solution at room temperature worsen (lower quantum yields and shorter excited-state lifetimes) upon introduction of phenyl groups on the ancillary ligand on going from complex **1** to **3**. Additionally, the absorption spectra recorded over time suggest that complex **3** presents a poor stability compared to **1** and **2**, likely due to a nucleophilic-assisted ancillary ligand-exchange reaction in the ground and/or in the excited states. The study of the dependence of the experimental intrinsic deactivation rate constant, $k_{in} = 1/\tau$, on the temperature, together with the theoretical characterization of the emitting (T_1) and metal-centered (^3MC) excited states, help to clarify the different photophysical behavior between complexes. Our results indicate that attachment of a phenyl group to the ancillary ligand (**2**) enhances the temperature-independent deactivation pathways, whereas attachment of a second phenyl group (**3**) also opens the temperature-dependent deactivation pathway through nonradiative ^3MC excited states. The enhancement of these deactivation pathways leads to poorer photoluminescent properties when going from complex **1** to **3** and is most likely the reason for the poor stability of **3**.

The study presented in this paper explains why LEC devices using complexes **2** and **3** are significantly less efficient than those based on **1**, since the efficacy of the device is ultimately related to the photophysical performance of the complex used as the active component.[72] The study also suggests that the thermal population of the nonradiative ^3MC states is the main reason for the lower amount of light emitted during the operation lifetime of the device by LECs built up using complex **3**.[21] For complexes **1** and **2**, the population of the ^3MC states in solution is not possible at room temperature. This does not automatically imply that this is also the case in solid-state electroluminescent devices as (a) the energy levels are characterized by a distribution of density of states (DOS) that reduces the energy differences between the electronic states and (b) the external bias applied generates a

polarization effect that also affects the relative energy of the states.

AUTHOR INFORMATION

Corresponding Author

*E-mail: gianluca.accorsi@isof.cnr.it (G.A.); enrique.orti@uv.es (E.O.).

Present Addresses

[§]Friedrich-Alexander-Universität Erlangen-Nürnberg, Department of Chemistry and Pharmacy & Interdisciplinary Center for Molecular Materials (ICMM), Egerlandstrasse 3, 91058 Erlangen, Germany.

ACKNOWLEDGMENT

This work has been supported by the European Union (CELLO, STRP 248043; ITN FINELUMEN, PITN-GA-2008-215399), the Italian Ministry of Education (MIUR) (LUCI, FIRB RBIP0642YL; NODIS, FIRB RBIP0642YL), the Italian National Research Council (CNR) (MACOL, PM.P04.010), and the Spanish Ministry of Science and Innovation (MICINN) (MAT2007-61584, CSD2007-00010, and CTQ2009-08790). R.D.C. acknowledges the support of the MICINN and the Alexander von Humboldt Foundation. A.B. and G.A. thank their colleague Francesco Barigelletti for helpful discussion during the preparation of the manuscript and Andrea Visentin for the technical support.

REFERENCES

(1) Balzani, V.; Campagna, S. *Photochemistry and Photophysics of Coordination Compounds I and II*; Springer: Berlin, Heidelberg, New York, 2007; Vol. 280.

(2) Ulbricht, C.; Beyer, B.; Friebe, C.; Winter, A.; Schubert, U. S. *Adv. Mater.* **2009**, *21*, 4418.

(3) Montalti, M.; Credi, A.; Prodi, L.; Gandolfi, M. T. *Handbook of Photochemistry*, 3rd ed.; Taylor & Francis: New York, 2006.

(4) Zhao, Q.; Liu, S.; Li, F. Y.; Yi, T.; Huang, C. H. *Dalton Trans.* **2008**, 3836.

(5) Schmittel, M.; Lin, H. W. *Inorg. Chem.* **2007**, *46*, 9139.

(6) Brandel, J.; Sairenji, M.; Ichikawa, K.; Nabeshima, T. *Chem. Commun.* **2010**, *46*, 3958.

(7) Borisov, S. M.; Klimant, I. *Anal. Chem.* **2007**, *79*, 7501.

(8) Slinker, J.; Bernards, D.; Houston, P. L.; Abruña, H. D.; Bernhard, S.; Malliaras, G. G. *Chem. Commun.* **2003**, 2392.

(9) Slinker, J. D.; Rivnay, J.; Moskowitz, J. S.; Parker, J. B.; Bernhard, S.; Abruña, H. D.; Malliaras, G. G. *J. Mat. Chem.* **2007**, *17*, 2976.

(10) Mullen, K.; Scherf, U. *Organic Light Emitting-Devices: Synthesis, Properties and Applications*; Wiley-VCH: Weinheim, 2006.

(11) Yersin, H. *Transition Metal and Rare Earth Compounds. Excited States, Transitions, and Interactions*; Springer-Verlag: Berlin, 2004; Vol. III.

(12) Maness, K. M.; Terrill, R. H.; Meyer, T. J.; Murray, R. W.; Wightman, R. M. *J. Am. Chem. Soc.* **1996**, *118*, 10609.

(13) Maness, K. M.; Masui, H.; Murray, R. W.; Wightman, R. M. *J. Am. Chem. Soc.* **1997**, *119*, 3987.

(14) Slinker, J. D.; Gorodetsky, A. A.; Lowry, M. S.; Wang, J.; Parker, S.; Rohl, R.; Bernhard, S.; Malliaras, G. G. *J. Am. Chem. Soc.* **2004**, *126*, 2763.

(15) Bolink, H. J.; Coronado, E.; Costa, R. D.; Ortí, E.; Sessolo, M.; Graber, S.; Doyle, K.; Neuburger, M.; Housecroft, C. E.; Constable, E. C. *Adv. Mater.* **2008**, *20*, 3910.

(16) Graber, S.; Doyle, K.; Neuburger, M.; Housecroft, C. E.; Constable, E. C.; Costa, R. D.; Ortí, E.; Repetto, D.; Bolink, H. J. *J. Am. Chem. Soc.* **2008**, *130*, 14944.

(17) He, L.; Duan, L.; Qiao, J.; Wang, R.; Wei, P.; Wang, L.; Qiu, Y. *Adv. Funct. Mater.* **2008**, *18*, 2123.

(18) Su, H.-C.; Chen, H.-F.; Wu, C.-C.; Wong, K.-T. *Chem. Asian J.* **2008**, *3*, 1922.

(19) Zysman-Colman, E.; Slinker, J. D.; Parker, J. B.; Malliaras, G. G.; Bernhard, S. *Chem. Mater.* **2008**, *20*, 388.

(20) Costa, R. D.; Céspedes-Guirao, F. J.; Ortí, E.; Bolink, H. J.; Gierschner, J.; Fernández-Lázaro, F.; Sastre-Santos, A. *Chem. Commun.* **2009**, 3886.

(21) Costa, R. D.; Ortí, E.; Bolink, H. J.; Graber, S.; Housecroft, C. E.; Neuburger, M.; Schaffner, S.; Constable, E. C. *Chem. Commun.* **2009**, 2029.

(22) Costa, R. D.; Ortí, E.; Bolink, H. J.; Graber, S.; Schaffner, S.; Neuburger, M.; Housecroft, C. E.; Constable, E. C. *Adv. Funct. Mater.* **2009**, *19*, 3456.

(23) He, L.; Qiao, J.; Duan, L.; Dong, G.; Zhang, D.; Wang, L.; Qiu, Y. *Adv. Funct. Mater.* **2009**, *19*, 2950.

(24) Kwon, T.-H.; Oh, Y. H.; Shin, I.-S.; Hong, J.-I. *Adv. Funct. Mater.* **2009**, *19*, 711.

(25) Rothe, C.; Chiang, C.-J.; Jankus, V.; Abdullah, K.; Zeng, X.; Jitchati, R.; Batsanov, A. S.; Bryce, M. R.; Monkman, A. P. *Adv. Funct. Mater.* **2009**, *19*, 2038.

(26) Costa, R. D.; Ortí, E.; Bolink, H. J.; Graber, S.; Housecroft, C. E.; Constable, E. C. *Adv. Funct. Mater.* **2010**, *20*, 1511.

(27) Costa, R. D.; Ortí, E.; Bolink, H. J.; Graber, S.; Housecroft, C. E.; Constable, E. C. *J. Am. Chem. Soc.* **2010**, *132*, 5978.

(28) Costa, R. D.; Pertegás, A.; Ortí, E.; Bolink, H. J. *Chem. Mater.* **2010**, *22*, 1288.

(29) He, L.; Duan, L.; Qiao, J.; Dong, G.; Wang, L.; Qi, Y. *Chem. Mater.* **2010**, *22*, 3535.

(30) Mydlak, M.; Bizzarri, C.; Hartmann, D.; Sarfert, W.; Schmid, G.; De Cola, L. *Adv. Funct. Mater.* **2010**, *20*, 1812.

(31) Nobeshima, T.; Morimoto, T.; Nakamura, K.; Kobayashi, N. *J. Mater. Chem.* **2010**, *47*, 1063.

(32) Yang, C.-H.; Beltran, J.; Lemaur, V.; Cornil, J.; Hartmann, D.; Sarfert, W.; Frohlich, R.; Bizzarri, C.; De Cola, L. *Inorg. Chem.* **2010**, *49*, 9891.

(33) Costa, R. D.; Ortí, E.; Bolink, H. J.; Graber, S.; Housecroft, C. E.; Constable, E. C. *Chem. Commun.* **2011**, *47*, 3207.

(34) Costa, R. D.; Ortí, E.; Tordera, D.; Pertegás, A.; Bolink, H. J.; Graber, S.; Housecroft, C. E.; Sachno, L.; Neuburger, M.; Constable, E. C. *Adv. Ener. Materials* **2011**, *1*, 282.

(35) Lenes, M.; Garcia-Belmonte, G.; Tordera, D.; Pertegás, A.; Bisquert, J.; Bolink, H. J. *Adv. Funct. Mater.* **2011**, *21*, 1581.

(36) Bolink, H. J.; Coronado, E.; Costa, R. D.; Lardiés, N.; Ortí, E. *Inorg. Chem.* **2008**, *47*, 9149.

(37) Su, H. C.; Fang, F. C.; Hwu, T. Y.; Hsieh, H. H.; Chen, H.; Lee, G.; Peng, S.; Wong, K. T.; Wu, C. C. *Adv. Funct. Mater.* **2007**, *17*, 1019.

(38) Colombo, M. G.; Güdel, H. *Inorg. Chem.* **1993**, *32*, 3081.

(39) Colombo, M. G.; Hauser, A.; Güdel, H. *Inorg. Chem.* **1993**, *32*, 3088.

(40) De Angelis, F.; Fantacci, S.; Evans, N.; Klein, C.; Zakeeruddin, S. M.; Moser, J. E.; Kalyanasundaram, K.; Bolink, H. J.; Graetzel, M.; Nazeeruddin, M. K. *Inorg. Chem.* **2007**, *46*, 5989.

(41) Dragonetti, C.; Falciola, L.; Mussini, P.; Righetto, S.; Roberto, D.; Ugo, R.; Valore, A.; De Angelis, F.; Fantacci, S.; Sgamellotti, A.; Ramon, M.; Muccini, M. *Inorg. Chem.* **2007**, *46*, 8533.

(42) Neve, F.; Crispini, A.; Campagna, S.; Serroni, S. *Inorg. Chem.* **1999**, *38*, 2250.

(43) Neve, F.; Crispini, A.; Serroni, S.; Loiseau, F.; Campagna, S. *Inorg. Chem.* **2001**, *40*, 1093.

(44) Dragonetti, C.; Falciola, L.; Mussini, P.; Righetto, S.; Roberto, D.; Ugo, R.; Valore, A.; De Angelis, F.; Fantacci, S.; Sgamellotti, A.; Ramon, M.; Muccini, M. *Inorg. Chem.* **2007**, *46*, 8533–8547.

(45) Ladouceur, S.; Fortin, D.; Zysman-Colman, E. *Inorg. Chem.* **2010**, *49*, 5625.
(46) Demas, J. N.; Crosby, G. A. *J. Phys. Chem.* **1971**, *75*, 991.
(47) Nakamaru, K. *Bull. Chem. Soc. Jpn.* **1982**, *55*, 2697.
(48) De Mello, J. C.; Wittmann, H. F.; Friend, R. H. *Adv. Mater.* **1997**, *9*, 230–236.
(49) Frisch, M. J.; Trucks, G. W.; Schlegel, H. B.; Scuseria, G. E.; Robb, M. A.; Cheeseman, J. R.; Scalmani, G.; Barone, V.; Mennucci, B.; Petersson, G. A.; Nakatsuji, H.; Caricato, M.; Li, X.; Hratchian, H. P.; Izmaylov, A. F.; Bloino, J.; Zheng, G.; Sonnenberg, J. L.; Hada, M.; Ehara, M.; Toyota, K.; Fukuda, R.; Hasegawa, J.; Ishida, M.; Nakajima, T.; Honda, Y.; Kitao, O.; Nakai, H.; Vreven, T.; Montgomery, J., J. A.; ; Peralta, J. E.; Ogliaro, F.; Bearpark, M.; Heyd, J. J.; Brothers, E.; Kudin, K. N.; Staroverov, V. N.; Kobayashi, R.; Normand, J.; Raghavachari, K.; Rendell, A.; Burant, J. C.; Iyengar, S. S.; Tomasi, J.; Cossi, M.; Rega, N.; Millam, N. J.; Klene, M.; Knox, J. E.; Cross, J. B.; Bakken, V.; Adamo, C.; Jaramillo, J.; Gomperts, R.; Stratmann, R. E.; Yazyev, O.; Austin, A. J.; Cammi, R.; Pomelli, C.; Ochterski, J. W.; Martin, R. L.; Morokuma, K.; Zakrzewski, V. G.; Voth, G. A.; Salvador, P.; Dannenberg, J. J.; Dapprich, S.; Daniels, A. D.; Farkas, Ö.; Foresman, J. B.; Ortiz, J. V.; Cioslowski, J.; Fox, D. J. *Gaussian 09*, Revision A.1; Gaussian, Inc.: Wallingford, CT, 2009.
(50) Becke, A. D. *J. Chem. Phys.* **1988**, *88*, 2547.
(51) Becke, A. D. *Phys. Rev. A* **1988**, *38*, 3098.
(52) Becke, A. D. *J. Chem. Phys.* **1993**, *98*, 5648.
(53) Francl, M. M.; Pietro, W. J.; Hehre, W. J.; Binkley, J. S.; Gordon, M. S.; Defrees, D. J.; Pople, J. A. *J. Chem. Phys.* **1982**, *77*, 3654.
(54) Hay, P. J.; Wadt, W. R. *J. Chem. Phys.* **1985**, *82*, 299.
(55) Cramer, C. S.; Truhlar, D. G. *Solvent Effects and Chemical Reactivity*; Kluwer: Dordrecht, The Netherlands, 1996.
(56) Tomasi, J.; Persico, M. *Chem. Rev.* **1994**, *94*, 2027.
(57) Lowry, M. S.; Hudson, W. R.; Pascal, R. A.; Bernhard, S. *J. Am. Chem. Soc.* **2004**, *126*, 14129.
(58) Waern, J. B.; Desmarets, C.; Chamoreau, L.-M.; Amouri, H.; Barbieri, A.; Sabatini, C.; Ventura, B.; Barigellett, F. *Inorg. Chem.* **2008**, *47*, 3340.
(59) Polson, M.; Fracasso, S.; Bertolasi, V.; Ravaglia, M.; Scandola, F. *Inorg. Chem.* **2004**, *43*, 1950.
(60) Turro, N. J.; Ramamurthy, V.; Scaiano, J. C. *Principles of Molecular Photochemistry*; University Science Book, 2009.
(61) Sajoto, T.; Djurovich, I.; Tamayo, A. B.; Oxgaard, J.; Goddard, W. A.; Thompson, M. E. *J. Am. Chem. Soc.* **2009**, *131*, 9813.
(62) Goushi, K.; Brooks, J.; Brown, J. J.; Sasabe, H.; Adachi, C. *J. Photopolym. Sci. Technol.* **2006**, *19*, 181.
(63) Finkenzeller, W. J.; Stossel, P.; Yersin, H. *Chem. Phys. Lett.* **2004**, *397*, 289.
(64) Yang, L.; Okuda, F.; Kobayashi, K.; Nozaki, K.; Tanabe, Y.; Ishii, Y.; Haga, M. A. *Inorg. Chem.* **2008**, *47*, 7154.
(65) Caspar, J. V.; Meyer, T. J. *J. Phys. Chem.* **1983**, *87*, 952.
(66) Englman, R.; Jortner, J. *Mol. Phys.* **1970**, *18*, 145.
(67) Freed, K. F.; Jortner, J. *J. Chem. Phys.* **1970**, *52*, 6272.
(68) Armaroli, N.; Accorsi, G.; Cardinali, F.; Listorti, A. *Top. Curr. Chem.* **2007**, *280*, 69.
(69) Schaffner-Hamann, C.; von Zelewsky, A.; Barbieri, A.; Barigelletti, F.; Muller, G.; Riehl, J. P.; Neels, A. *J. Am. Chem. Soc.* **2004**, *126*, 9339.
(70) Barigelletti, F.; Juris, A.; Balzani, V.; Belser, P.; Vonzelewsky, A. *J. Phys. Chem.* **1987**, *91*, 1095.
(71) Alary, F.; Heully, J. L.; Bijeire, L.; Vicendo, P. *Inorg. Chem.* **2007**, *46*, 3154.
(72) Malliaras, G. G.; Scott, J. C. *J. Appl. Phys.* **1998**, *83*, 5399.